Review

Fluorinated and Non-Fluorinated Electro-Optic Copolymers: Determination of the Time and Temperature Stability of the Induced Electro-Optic Coefficient

Alessandro Belardini

Dipartimento di Scienze di Base ed Applicate per l'Ingegneria, Sapienza Università di Roma and CNISM/Via A. Scarpa 14, I-00161 Roma, Italy; E-Mail: alessandro.Belardini@uniroma1.it; Tel.: +39-06-4996-800; Fax: +39-06-4424-0183

Abstract: Organic fluorinated materials demonstrate their excellent electro-optic properties and versatility for technological applications. The partial substitution of hydrogen with fluorine in carbon-halides bounds allows the reduction of absorption losses at the telecommunication wavelengths. In these interesting compounds, the electro-optic coefficient was typically induced by a poling procedure. The magnitude and the time stability of the coefficient is an important issue to be investigated in order to compare copolymer species. Here, a review of different measurement techniques (such as nonlinear ellipsometry, second harmonic generation, temperature scanning and isothermal relaxation) was shown and applied to a variety of fluorinated and non-fluorinated electro-optic compounds.

Keywords: electro-optic polymers; fluorinated polymers; electro-optic time stability

1. Introduction

Organic conjugated polymers were thoroughly investigated in recent years due to their interesting and peculiar physical properties, granted by electron delocalization of the π-bonds. Moreover, the extraordinary physical properties shown by organics can be easily tuned by appropriate synthesis processes [1,2], providing a beneficial stimulus for applied research. In the last few decades, in particular, a great deal of effort was made to study the optical and electronic properties of organic copolymers. Electrical conductivity, nonlinear optical response, luminescence and electro-luminescence

in this class of materials were studied extensively. These studies culminated in the Nobel Prize awarded in 2000 to Heeger, MacDiarmid and Shirakawa for their discoveries on conjugated polymers that allowed to extend the results obtained in the field of inorganic semiconductor electronics and photonics to the field of organics.

Nowadays, organic materials have emerged from academic research to become useful building blocks of integrated optical devices for light emission, modulation and switching [3,4].

The large-scale introduction of optical technologies in communication networks has become a reality with an enormous impact on the bandwidth and quality of communication services offered, on the economy of the industrialized countries and also on interpersonal and social relations. Fiber optics has enabled high bit-rate transmission capacity in the core network. Broad-band access, however, is limited because of the high costs of the hardware needed for distributing, routing and switching and eventually generation and detection of the optical signals. Guided by the situation in the field of electronics, the solution should be found in large-scale integration of optical functions in compact optical circuitries. The conversion of source data that are mainly in the electrical domain to optical bits and the dynamical functionality in optical networks require electro-optic or other active optical materials. Hybrid integration of passive wave-guiding structures with these active materials is a route to low-cost, high-performance modules. In this context, progress in organic materials demonstrates the excellent electro-optic properties and versatility for technological applications, for example a polymeric electro-optic modulation, based on a Mach-Zehnder integrated interferometer (MZI) operating at over 200 GHz was demonstrated [5] or electro-optic modulators based on microring resonator design [6,7].

Among other advantages of organic materials, we can point out the compatibility with a variety of substrates, such as Si, GaAs, or plastics (a high-performance electro-optic polymer modulator on a flexible substrate was fabricated [8]), the ability to be efficiently integrated with very large scale integration (VLSI) semiconductor electronic circuitry, and the low-cost fabrication techniques. There are critical points that need improvement and are currently under study. Photo and thermal stability of the polymers increased with the synthesis of cross-linkable polymers [9,10] and high glass transition temperature (High-Tg) polymers [11]. Optical losses at the telecommunication wavelength of 1.3 μm and 1.55 μm due to absorption by carbon-hydrogen (C-H) vibrational overtones (typically exceeding 0.5 dB/cm at 1,300 nm and 1 dB/cm at 1,550 nm) was reduced to 0.1 dB/cm by substitution of the hydrogen with heavier halogens like fluorine that has the effect of shifting the overtone peaks to longer wavelengths [2,12].

Here we show a review of the characterization technique used in order to retrieve the magnitude and the thermostability of the electro-optic properties of different species of fluorinated and non-fluorinated polymers.

In the second section we briefly introduce the concept of second order susceptibility of molecules, the most frequently used orientation techniques that allow for obtainment of a macroscopic electro-optic response and the theoretical stability of the induced electro-optic coefficient.

In the third section, we review the main techniques used in order to measure the magnitude of the electro-optic response, namely the nonlinear ellipsometry or Teng and Man technique (NLE or TMT) [13–16] and second harmonic generation (SHG) [17–20], then we show how these techniques

can be used in order to evaluate the stability of the electro-optic response by performing temperature scanning measurements and isothermal relaxation measurements.

In the fourth section, we show how the previous techniques were applied in literature in order to retrieve the stability properties of different fluorinated and non-fluorinated copolymers.

2. Electro-Optic Properties of Polymers

2.1. Second Order Nonlinear Susceptibility

In many applications and in a more realistic description of the electromagnetic interaction, the response of a medium immersed in an electromagnetic field cannot be described as a linear response:

$$P_i = \varepsilon_0 \, \chi_{ij} \cdot E_j \tag{1}$$

(*i.e.*, by considering that the dielectric susceptibility of the material is not dependent on the amplitude of the electric field). A more complete description of the electric polarization can be expressed in a general way as [17,21]:

$$\vec{P} = \vec{f}(\vec{E}) \tag{2}$$

Such dependence can be expanded in a power series of the electric field, and in a general case the electric polarization vector can be written as [17]:

$$P_i = \varepsilon_0 \left(\chi_{ij}^{(1)} E_j + \chi_{ijk}^{(2)} E_j E_k + \chi_{ijkl}^{(3)} E_j E_k E_l + \ldots \right) \tag{3}$$

where the nonlinear susceptivities $\chi^{(n)}$ are used (the $\chi^{(1)}$ term is responsible for the linear refractive index). In centrosymmetric materials are present only the even term of Equation (3), otherwise in non-centrosymmetric materials the second order term $\chi^{(2)}$ can be dominant with respect to the other nonlinear terms.

We limit our attention only at the second order term that is responsible of the linear electro-optic (EO) effect (or Pockels effect) as well as other interesting phenomena and applications such as second harmonic generation (SHG), frequency mixing, photorefractivity [17,22].

In Equation (3) if we consider that the driving field oscillates at one frequency ω, the only possible effects in the polarization term P are second harmonic generation (where P oscillates at 2ω) and optical rectification (where the solution with P that oscillates at $\omega = 0$ means that a static field results to be applied at the material when it is shined by the light).

If the exciting field is composed by an electromagnetic field oscillating at $\omega_1 = \omega$ and an external static electric field that is applied to the material ($\omega_2 = 0$), the resulting polarization P oscillates with the same frequency ω of the incident electromagnetic field, like in the case of the linear term $\chi^{(1)}$, but the linear term responsible for the refractive index is modified by the presence of the static field:

$$P_i^\omega = \varepsilon_0 \chi_{ij}^{(1)} E_j^\omega + \varepsilon_0 \chi_{ijk}^{(2)} E_j^\omega E_k^0 = \varepsilon_0 \left(\chi_{ij}^{(1)} + \chi_{ijk}^{(2)} E_k^0 \right) E_j^\omega \tag{4}$$

This phenomenon is the EO effect of our interest.

2.2. Electro-Optic Properties of a Single Molecule

Organic conjugated molecules and polymers show interesting and peculiar physical properties, given by electron delocalization of the π-bonds [1]. If we consider benzene (C_6H_6), it shows complete delocalization of π-electrons on the aromatic ring (Figure 1(a)). As we saw in the previous chapter, as benzene is a nonpolar molecule and it is centrosymmetric, it does not show any second order nonlinear contribution to the polarization term.

Figure 1. (**a**) Centrosymmetric benzene. (**b, c**) Non-centrosymmetric donor acceptor substituted benzenes.

(**a**)   (**b**)   (**c**)
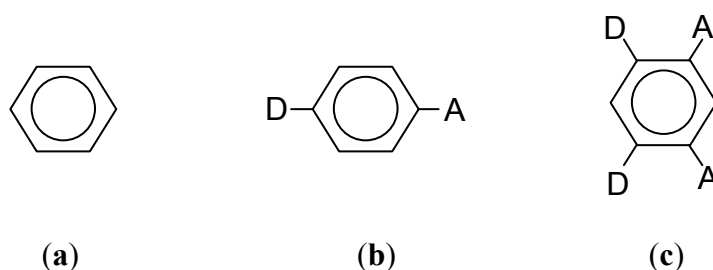
If we substitute some hydrogen atoms with an electron acceptor A (for example NO_2) or electron donor group D (for example NH_2) (Figure 1(b,c)), the benzene ring allows the electrical charges to flow from the donor to the acceptor, generating a dipole moment along the conjugation direction. We can expect that non-centrosymmetric molecules, with large mobility of charges will show a large degree of polarization and nonlinear optical terms, especially of the second order.

For a general molecule, using a description similar to that used in the previous paragraph for macroscopic nonlinear media, we can write down the expression of the induced dipole moment as:

$$\mu_i = \mu_{0i} + \varepsilon_0 \alpha_{ij} F_j + \varepsilon_0 \beta_{ijk} F_j F_k + \varepsilon_0 \gamma_{ijkl} F_j F_k F_l + \dots \qquad i,j,k,l = 1,2,3 \qquad (5)$$

where μ_{0i} are the static electric dipole moment components, α_{ij} are the polarizability tensor components, β_{ijk} and γ_{ijkl} are the components of the hyperpolarizabilities tensors of the first and second order, respectively, and finally F_i represent the *i* components of the local electric field $\vec{F}$ that is related to the macroscopic electric field $\vec{E}$ by the local field factor f^ω via the following relation:

$$\vec{F} = f^\omega \vec{E} \qquad (6)$$

The local field factor in the range of the optical frequencies is given by the Lorenz-Lorentz formula:

$$f^\omega = \frac{n^2(\omega) + 2}{3} \qquad (7)$$

where $n(\omega)$ is the refractive index at ω. For static fields, the field factor is given by the Onsager expression:

$$f^0 = \frac{\varepsilon_{r0}(\varepsilon_{r\infty} + 2)}{\varepsilon_{r\infty} + 2\varepsilon_{r0}} \qquad (8)$$

where ε_{r0} is the static relative dielectric constant and $\varepsilon_{r\infty}$ is the relative dielectric constant in the range of optical frequencies [12,23].

One of the best known electro-optic chromophore used in applications is the 4-[*N*-ethyl-*N*-(2-hydroxyethyl)]amino-4'-nitroazobenzene (Disperse Red 1; DR1), whose structure is shown in Figure 2(a).

Figure 2. (**a**) Chemical structure of the Disperse Red 1 (DR1) and (**b**) of the (poly)-methyl-metha-acrylate (PMMA).

(**a**)   (**b**)
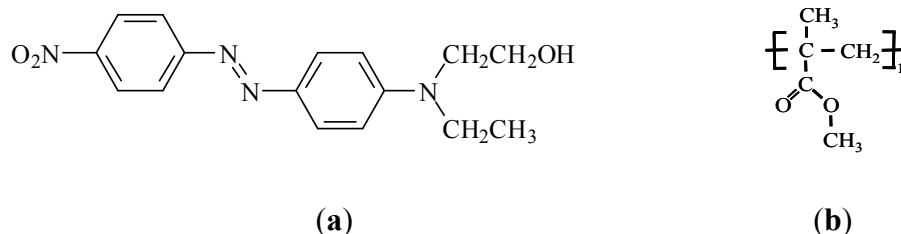
The main characteristics are reported in Table 1 [12,24–29]. A comparison between electrostatic units (esu) and International System units (SI), is given in [30].

Table 1. Characteristic data of the Disperse Red 1 (DR1) molecule.

Chromophore	λ_{max} (nm, CHCl$_3$)	μ_0 (Debye)	β_0 (10^{-30} esu)	$\beta_{1.9\mu m}$ (10^{-30} esu)	$\mu_0\beta_{1.9\mu m}$ (10^{-48} esu)
DR1	480 (497)	7.7 (8.7)	40	5,046	580

2.3. Inducing of the Macroscopic Electro-Optic Properties

Up to now, we described the nonlinear optical properties of a single molecule. However we are generally interested to the nonlinear optical response of bulk macroscopic materials made out of a large number of such molecules.

In order to evaluate the nonlinear response of the whole macroscopic material it is not sufficient to know the nonlinear properties of the single molecule, but we need to consider the number of chromophores per volume unit and their orientation inside the macroscopic structure. In particular, the macroscopic nonlinear optical properties increase with the density of oriented chromophores. Considering a system constituted by molecules with large β, if they are isotropically oriented in the space, the macroscopic second order dielectric susceptibility $\chi^{(2)}$ is zero because the material, as a whole, is centrosymmetric.

Since we are interested in electro-optic applications, we need to achieve a high $\chi^{(2)}$ value and consequently we need to fabricate a structure in which the nonlinear molecules are oriented in a polar order. One way is to realize a solid solution of highly nonlinear molecules in a high optical quality passive polymer matrix. The matrix, in order not to interfere with the optical properties of the chromophore, is in general transparent in the wavelength used for applications and can be considered as optically linear; it is just a host material that gives mechanical stability to the ensemble of nonlinear molecules. One of the most used polymer matrices is the poly-methyl-metha-acrylate (PMMA) [12] whose chemical structure is shown in Figure 2(b). Usually, the material is deposited onto different types of substrates by spin-coating, producing amorphous thick films (1~2 μm). The chromophores,

randomly oriented at the end of the film deposition procedure, must be aligned in a non-centrosymmetric fashion after deposition by means of a poling procedure, as we shall describe later.

There are several ways of introducing nonlinear optical chromophores into the polymer matrix. The two most common methods are dissolving (guest-host systems) and covalently attaching (functionalized system) the chromophores to the polymer.

In the guest-host system, nonlinear optic (NLO) chromophores are dissolved, in the polymer host. The principal disadvantages of such a structure are: (i) low nonlinear activity, that it is due to the dopant maximum solubility (largest concentration is about 10% of the host weight), because greater concentrations can lead to chromophores' aggregation or crystallization; (ii) the presence of optical losses due to scattering originated by the non homogeneity of the structure; (iii) the thermal and temporal instability, in fact, the chromophores are not attached at the polymer matrix and they can move with a higher degree of freedom. In the functionalized systems, the chromophores are attached to the polymer matrix, and the relative dopant concentration can be much higher than in guest-host systems. Moreover functionalized systems are more stable since their orientational mobility is significantly hindered and the order of such systems therefore relaxes more slowly.

In the functionalized systems nonlinear optical chromophores can be incorporated in the polymer matrix by chemically attaching them into the polymer main-chain (or backbone) or as a pendant side-group. In the side-chain systems, the chromophores can rotate around the attaching point and it is easier to orient them in the poling procedure. Nevertheless, the orientation is maintained longer than in the guest-host systems. For all these reasons, side-chain copolymers are widely used in optical application but also guest-host systems are used because of the relatively easy fabrication process.

In order to induce non-centrosymmetry after the films deposition, several poling techniques can be used. The most common ones are:

Contact Poling or *Electrode Poling*. Chromophores such as DR1 show a large static dipole moment μ_0, due to their rod shape with donor and acceptor at the opposite sides. As a result, it is possible to use a large static electric field to orient these polar molecules along the field and thus induce an asymmetric configuration. For contact poling, the sample must be prepared by spinning the polymeric solution on a substrate that was previously covered by an electrode. Then, after spinning and drying, the polymeric film must be topped with another electrode, via sputtering deposition or other techniques, in order to obtain a sandwich structure with the copolymer sandwiched between the two electrodes. Then, the sample is ready for the poling procedure; the temperature of the sample is increased to the glass transition one (T_g), where the polymer matrix reaches a large mobility. A large static electric field is then applied between the two electrodes for a sufficient time, in order to align the nonlinear molecules; then with the field still on, the temperature is slowly decreased to Room Temperature and the field is subsequently removed. At Room Temperature the orientational mobility of the molecules is sufficiently low to maintain the chromophores alignment for a long time and consequently giving rise to a long lasting electro-optic coefficient. With such a method it is not possible to apply a very large field, because unavoidable small imperfections in the polymer film can lead to a decrease of the dielectric rigidity of the material and, as a consequence to electrical discharge with complete damage of the sample.

Corona Poling. In such a technique [23] it is not necessary to apply electrodes on the polymeric material, as a consequence, it is possible for example to deposit, by spin coating, a polymeric film

directly on a bare substrate. In the corona poling procedure the sample is put on a metal plate that plays simultaneously the role of heater and bottom electrode. The top electrode is given by a layer of ions which are deposited on the film surface. In order to produce the ions, a tungsten needle is placed near the surface of the polymer film at a potential of about 1–10 kV with respect to the substrate. The needle generates an intense electric field that ionizes the surrounding atmosphere (usually an inert gas, nitrogen, for example) and the generated ions are pushed on the film surface where they accumulate. As a consequence, the charges produce a quite uniform high intense field that orients the nonlinear dipoles. As in the case of electrode poling, the temperature is increased close to T_g for a suitable time interval during the poling procedure, then it is lowered to Room Temperature, still maintaining the voltage drop between needle and substrate. Corona poling is more efficient than electrode poling because it can generate very intense fields. Also during corona poling procedure, there is the possibility of having electrical discharge due to the high field, but in this case, since the ions are not mobile on the surface of the material, the discharges are localized and the sample does not damage the whole surface.

The method is, however, the subject of criticism for material characterization purposes: in fact, the real effective poling field remains unknown and it is not well reproducible.

Photoassisted Poling. In the previously described techniques it is necessary to pole the sample at a high temperature in order to have sufficient chromophore mobility. Nevertheless, at high temperatures, there is a competition between the alignment effect of the electric field and, on the other side, the thermal motion of the molecules. For high-T_g copolymers, poling samples with such techniques can lead to low efficiency. The advantage of photoassisted poling [31,32] is that this procedure can be executed also at room temperature. The sample is prepared as in the electrode poling, with the polymer sandwiched between two electrodes, but in this case at least one of the electrodes must be transparent. During poling, a voltage drop is applied between the two electrodes. Meanwhile, the sample is shined, from the transparent electrode side, by a light beam which wavelength is tuned in the region of the absorption resonance of the chromophore. In conjugated molecules with a N=N bridge along the principal axis, as DR1, the light, with a suitable polarization state, is absorbed by the chromophores and produces a trans-cis-trans isomerization (Figure 3). After several *trans-cis-trans* cycles, a net centrosymmetric orientation of the dipoles perpendicular to the pump light field can be achieved. With additionally applied dc electric poling fields, the process permits non-centrosymmetric orientation of chromophores giving rise to a macroscopic electro-optic coefficient even at room temperature.

Figure 3. Photoassisted poling.
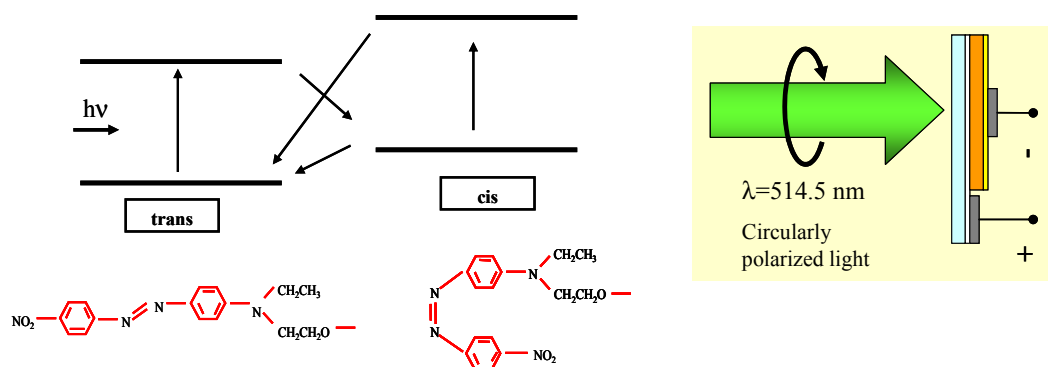
In all the three cases described above, the electro-optic coefficient induced by poling will relax on a long-time scale, because the chromophores' orientational mobility is not zero, even at room temperature.

2.4. Steady-State Properties of the Induced Electo-Optic Coefficient

In this paragraph, we show a theoretical model describing the nonlinear optical response of a medium constituted by nonlinear units (chromophores) dispersed in a linear matrix and oriented along a preferential axis [33,34]. We suppose that each molecule is identified by an intrinsic reference system with the axes named 1, 2, 3, and this system can be rotated in respect to the system that describes the whole macroscopic structure with the axes named x, y, z (laboratory axis). Let us consider that the orientation of the nonlinear molecules is described by a statistical angular distribution function $f(\Omega) = f(\theta, \varphi)$ of the molecular axes, where θ and φ are shown in Figure 4. $f(\Omega)$ must fulfill the normalization condition $\int_\Omega f(\Omega) d\Omega = 1$. In the following we consider that z is the direction of the poling field and 3 is the direction of the long axis of the molecule.

Figure 4. Relationship between the molecular axes 1,2,3 and laboratory axes x,y,z.
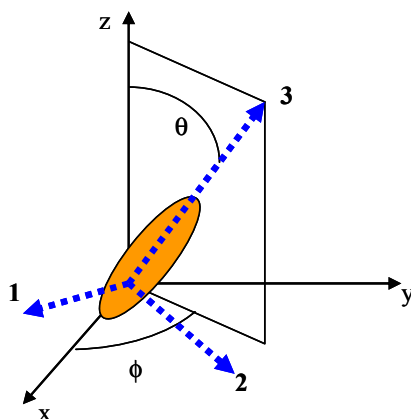
The second order nonlinear dipole moment results in:

$$p_i^\omega = \varepsilon_0 \beta_{ijk}(-\omega, \omega, 0) f^\omega f^0 E_j^\omega \cdot E_k^o \tag{9}$$

Considering the cylindrical and elongated shape of the chromophores, we can assume that the only nonvanishing component of β_{ijk} is β_{333}.

The macroscopic electro-optic polarization induced by an external dc field $\vec{E}^0 = E_z^0 \hat{z}$ and by an optical field $\vec{E}^\omega = E_z^\omega \hat{z}$, both of them along the z direction, is:

$$\begin{aligned}
P_z^\omega &= N \int p_3^\omega \cos(3, z) f(\Omega) d\Omega = \\
&= \varepsilon_0 \left[N f^0 f^\omega \int \beta_{333}(-\omega, \omega, 0) \cos^3(3, z) f(\Omega) d\Omega \right] E_z^\omega E_z^0
\end{aligned} \tag{10}$$

where

$$f(\Omega) = \frac{\exp\left(-\dfrac{U}{kT}\right)}{\displaystyle\int_\Omega \exp\left(-\dfrac{U}{kT}\right) d\Omega} \propto \exp\left(-\frac{U}{kT}\right) \tag{11}$$

and $\cos(\hat{i}, \hat{j})$ is the) cosine of the angle formed by the two directions $\hat{i}$, $\hat{j}$.

In order to find another component of the macroscopic nonlinear optical susceptibility, we consider the case where the external dc field is along the z direction, and the external optical field is along the x direction, $\vec{E}^{\omega} = E_x^{\omega} \hat{x}$. In this case, the electro-optic susceptibility can be obtained by considering the induced polarization along the x direction:

$$
\begin{aligned}
P_x^{\omega} &= N \int p_3^{\omega} \cos(3, x) f(\Omega) d\Omega = \\
&= \varepsilon_0 \left[N f^0 f^{\omega} \int \beta_{333}(-\omega; \omega, 0) \cos^2(3, x) \cos(3, z) f(\Omega) d\Omega \right] E_x^{\omega} E_z^0
\end{aligned}
\tag{12}
$$

From the above relations we obtain the following relations for the macroscopic electro-optic susceptibility:

$$
\chi_{zzz}^{(2)}(-\omega; \omega, 0) = N f^0 f^{\omega} \int \beta_{333}(-\omega; \omega, 0) \cos^3(3, z) f(\Omega) d\Omega
\tag{13}
$$

$$
\chi_{xxz}^{(2)}(-\omega; \omega, 0) = N f^0 f^{\omega} \int \beta_{333}(-\omega; \omega, 0) \cos^2(3, x) \cos(3, z) f(\Omega) d\Omega
\tag{14}
$$

During poling, two competing mechanisms determine the final steady-state equilibrium distribution. The electric dipole interaction of the molecular dipoles with the dc field favors the alignment of molecular dipoles along the z direction, while the thermal agitation tries to disorient the dipoles, leading to the maximum entropy configuration. For a sufficiently high temperature (even room temperature is high enough), the statistical distribution follows, as we said before, a Boltzmann distribution Equation (11): $f(\Omega) \propto \exp(-U/kT)$. The dipole interaction energy is given in the weak poling approximation by $f(\theta) \propto \exp(-U/kT) = \exp[x \cos(\theta)]$ where $x = \dfrac{\mu_0 f^0 E_p}{kT}$ with $x = (\mu_0 f^0 E_p / kT) \ll 1$.

This expression allows to estimate directly the second order susceptibility terms from Equations (13) and (14):

$$
\chi_{zzz}^{(2)}(-\omega; \omega, 0) = N f^0 f^{\omega} \beta_{333}(-\omega; \omega, 0) \mu_0 f^0 E_p / 5kT
$$
$$
\chi_{xxz}^{(2)}(-\omega; \omega, 0) = N f^0 f^{\omega} \beta_{333}(-\omega; \omega, 0) \mu_0 f^0 E_p / 15kT
\tag{15}
$$

The Equation (15) give, also, a first order approximation of the ratio $\chi_{zzz}^{(2)} / \chi_{xxz}^{(2)}$, that results in:

$$
\frac{\chi_{zzz}^{(2)}}{\chi_{xxz}^{(2)}} = 3
\tag{16}
$$

By applying the relation between the electro-optic tensor with the $\chi^{(2)}$ tensor [16], it is possible to apply the previous relations (15–16) to the electro-optic coefficient too.

$$
r_{ij}(-\omega; \omega, 0) = -\frac{2}{n_i^4} \chi_{iij}^{(2)}(-\omega; \omega, 0)
\tag{17}
$$

The calculations previously exposed neglect the chromophore–chromophore intermolecular electrostatic interactions. In this regime the electro-optic coefficient will increase in a linear manner with chromophore number density N (loading) in the host polymer matrix. More realistically, if the chromophore density is high enough, the reciprocal average distance between two nonlinear molecules, is so close to not allow neglecting of electrostatic interaction between the chromophores. Since the chromophores are polar molecules with a static dipole moment μ_0, they will interact, thereby

minimizing their energy and forming an anti-ferroelectric state, where neighbouring chromophores are preferentially oriented in opposite directions, leading to a decrease of the effective electro-optic coefficient [27]. In order to avoid the negative interaction between chromophores, non-polar second order nonlinear molecule were proposed [35]. Unfortunately, in these molecules, since they have no μ_0, it is not possible to align them using the standard poling procedure shown previously. A more complicated all-optical poling was proposed [35].

2.5. Transient Properties

At the end of the poling procedure, when temperature has been lowered to the ambient one and the poling field has been turned off, the orientational distribution $f(\Omega)$ is no longer at thermodynamic equilibrium and will relax via an orientational diffusion process, slowly decreasing the magnitude of the induced electro-optic properties. The distribution function is then time-dependent $f(\Omega, t) = f(\theta, t)$. The same happens if we consider the inverse problem, when an isotropic material is subject, since a certain time, to a poling field.

In order to describe these time-dependent phenomena, we introduce the rotational diffusion equation (Smoluchowski-Einstein) for a molecular dipole [33]:

$$\frac{1}{D}\frac{\partial f(\theta,t)}{\partial t} = \frac{1}{\sin(\theta)}\frac{\partial}{\partial \theta}\left\{\sin(\theta)\left[\frac{\partial}{\partial \theta}f(\theta,t) + \frac{1}{kT}\frac{\partial U}{\partial \theta}f(\theta,t)\right]\right\} \quad (18)$$

where D is a diffusion constant, related to the orientational mobility of the nonlinear dipoles in the polymer matrix.

However the behavior expected from the model showed above is not always in strong agreement with experimental data, because in the model, it is assumed that the material homogeneously acts on the mobility of the chromophores via a determined diffusion constant D. In reality, the polymer matrix is an amorphous inhomogeneous medium and each chromophore feels a different environment with a own diffusion constant D_i. The values of the diffusion constants are statistically distributed with a mean value and variance. For example in the guest-host system the chromophores manly feel two time constants [36], the faster one due to the rotation of the single chormophores around their original position, while the slowest one is due to the relaxation of the polymer host matrix. In side-chain polymers, usually we do not observe a single or double time constant exponential relaxation, but a stretched exponential with a homogeneous distribution of time constants with a given spread. In this case, in order to describe the time dependence of the electro-optic coefficient for an inhomogeneous matrix, the following expression is often used:

$$r_{zz}(t) = r_{zz}(\infty) + \Delta r_{zz}(E_p) \cdot \Phi(t) \quad (19)$$

where $r_{zz}(\infty)$ is the steady-state electro-optic response, $\Delta r_{zz}(E_p)$ is the induced electro-optic coefficient for a poling field E_p and $\Phi(t)$ is the Kohlrausch-Williams-Watts (KWW) stretched exponential function given by [37–39]:

$$\Phi(t) = \exp\left[-\left(\frac{t}{\tau}\right)^{\beta}\right] \quad (20)$$

Where β is a stretching parameter describing the deviation from the simple exponential law. The value of β is always between 0 and 1, where 0 represents a wide distribution of time constants and 1 represents a Dirac delta distribution leading to a single exponential relaxation, representative of the Debye model. For $\beta \neq 1$, the τ time constant alone is not meaningful and its average must be taken into account:

$$\langle \tau \rangle = \int_0^\infty \exp\left[-\left(\frac{t}{\tau}\right)^\beta\right] dt = \frac{\tau \Gamma(1/\beta)}{\beta} \tag{21}$$

where $\Gamma(x)$ is the Euler gamma-function $\Gamma(x) = \int_0^{+\infty} t^{x-1} e^{-t} dt$.

The average time constant $<\tau>$ depends on temperature with different laws:

For temperature above or equal to T_0, a characteristic temperature of the material that is close to, but lower than, the glass transition, the matrix is in a quasi-fluid state and the chromophores can move easily. In this case, the time constant follows the Vogel-Fulcher-Tamann-Hesse (VFTH) or Williams-Landel-Ferry (WLF) law that is typical of semi-fluid glassy systems:

$$\log\left[\frac{\langle \tau \rangle}{\langle \tau_o \rangle}\right] = \frac{B}{T - T_o} \tag{22}$$

where B is a suitable constant.

For temperatures below T_0, the average time constant follows an Arrhenius behavior:

$$\log\left[\frac{\langle \tau \rangle}{\langle \tau_o \rangle}\right] = \frac{E_a}{RT} \tag{23}$$

where E_a is the activation energy of the process and R is the universal gas constant ($R = K_B N_a = 8.31447$ J·mol^{-1}·K^{-1}).

Also β depends on temperature, as it is related to dipole mobility. It was shown that its dependence on temperature can be heuristically described by the expression [31]:

$$\beta(T) = \beta_0 + \frac{1 - \beta_0}{2}\left[1 - \tanh\left(\frac{A}{R} \frac{T_\beta - T}{T_\beta T}\right)\right] \tag{24}$$

where β_0, T_β and A are suitable constants.

3. Measurement Techniques of the Electro-Optic Coefficient

3.1. Nonlinear Ellipsometry

Nonlinear ellipsometry (NLE) is based on a single wavelength reflection configuration proposed, independently, by Teng and Man [13] and Schildkraut [14] in 1990. Since its introduction, the Teng and Man technique (TMT) has been widely used for the determination of the electro-optic susceptibility of organic polymer films and it demonstrated to be sensitive to a number of contributions to the measured signals that can lead to the evaluation of several nonlinear parameters [1,40,41]. The TMT permits the measurement of both $\tilde{\chi}^{(2)}(-\omega;\omega,0)$ and $\tilde{\chi}^{(3)}(-\omega;\omega,0,0)$ [42] complex susceptibilities.

Moreover, it is sensitive to space distributions of charges trapped in the polymer films [1,16,43]. In order to be applied, the TMT needs to operate on samples in which the polymer film is sandwiched between two electrodes. In the case of polymers for $\chi^{(2)}$ applications, the two electrodes are used either to pole the film or to apply a modulating voltage on the polymer film itself in order to measure the $\chi^{(2)}$ values. As the TMT is based on the measurement of the electric field induced change of the optical phase difference experienced by the s (perpendicular to the incidence plane) and p (parallel to the incidence plane) components of a laser which propagates through the polymer film, at least one (reflection operation) of the electrodes must be transparent to the probe light.

Usually, a semiconductive transparent oxide thin layer, deposited on a glass substrate is used as transparent electrode. A polymer film is then deposited by spin coating it and then coating it with a metal electrode. Some researchers used polymer films sandwiched between two transparent electrodes and performed the experiments in a transmittance configuration [44,45]; in this case the samples were produced by spin coating pairs of polymer films onto oxide coated glass slides and then sandwiching them face to face; elimination of the air gap was guaranteed by baking at glass transition temperature under mechanical pressure.

The experimental configuration in reflection mode for TMT is usually composed by a cw laser that impinges on the sample at an incident angle α after passing through a polarizer, which sets its polarization at 45° with respect to the incidence plane, and a phase compensating device that changes the relative phase between the s and p components of the laser beam by an amount ψ_c. After reflection at the polymer-metal interface, the beam is analyzed by a polarizer that is crossed with respect to the input one. The power of the beam transmitted by the whole system is detected by a photodiode. Between the electrodes it is applied either a dc voltage V_p during the poling procedure, or a modulated voltage $V(t)$ during the measurement of the electro-optic coefficient, given by:

$$V(t) = V_m \cos(\Omega t) \qquad \text{with } \Omega << \omega \tag{25}$$

The optical power at the output of the whole system is modulated, due to the response of the polymer film, both at Ω and 2Ω through the linear $\chi^{(2)}$ and quadratic $\chi^{(3)}$ electro-optic response.

The average output power can be written as:

$$P_{dc} = \tfrac{1}{4} P_0 |r_s|^2 \left[1 + (\tan\Phi)^2 - 2\tan\Phi \cdot \cos(\Psi_{ps} + \Psi_c) \right] \tag{26}$$

where P_0 is the input beam power after the first polarizer, ψ_{ps} and ψ_c are the phase differences between s and p polarizations originated by the propagation of the light in the polymer and in the phase compensator, respectively. Φ is defined by the ellipsometry relation

$$\frac{r_p}{r_s} = e^{j\Psi_{ps}} \cdot \tan\Phi \tag{27}$$

where and r_p and r_s are the Fresnel field reflection coefficients for the p and s polarization, respectively.

In the low birefringence approximation, with the assumption of $\Delta|r_s|^2 \approx 0$, the amplitude of the P_{ac} component at Ω is given by:

$$P_{ac}(\Omega) = \frac{k_0}{n^2} \frac{\sin^2(\alpha)}{\sqrt{n^2 - \sin^2\alpha}} P_0 |r_s|^2 \cdot V_m \cdot$$

$$\cdot \left\{ \mathrm{Re}\left(\chi_{333}^{(2)} - \chi_{113}^{(2)}\right) \cdot \sin(\Psi_{ps} + \Psi_c) \cdot + \mathrm{Im}\left(\chi_{333}^{(2)} - \chi_{113}^{(2)}\right) \left[\tan\Phi - \cos(\Psi_{ps} + \Psi_c) \right] \right\} \tag{28}$$

with $\chi_{333}^{(2)} = 3\chi_{113}^{(2)}$ in the weak poling approximation.

By varying the phase difference ψ_c introduced by the compensator from 0 to 2π, Equations (26) and (28) give the parametric equations of an ellipse.

There are two working points (labeled 1 and 2) where the P_{dc} reach half of its maximum value: $P_{dc}^{(1,2)} = \frac{1}{2} P_{dc\,max}$. Those conditions can be found when: $\Psi = \Psi_{ps} + \Psi_c = \pm \pi/2$.

By using a lock-in amplifier, it is possible to measure the effective P_{ac} signal in these two working points and then it is possible to retrieve the electro-optic coefficient by the relation:

$$r_{33} = \frac{3\lambda_0}{2\pi} \cdot \sqrt{2} \cdot \frac{\sqrt{n^2 - \sin^2 \alpha}}{n^2 \sin^2 \alpha} \cdot \frac{P_{ac}^{(1,eff)} - P_{ac}^{(2,eff)}}{4 P_{dc}^{(1,2)}} \cdot \frac{1}{V_m} = 3 r_{13} \tag{29}$$

We point out that the measurements in the two working points 1 and 2 are faster than the measurement based on the sampling of the whole ellipse, but suffer from lower accuracy. The faster measurements can be usefully adopted in monitoring the time decay of the electro-optic coefficient, as we will show later.

Usually, when analyzing experimental data in an ellipsometric measurement, one makes the assumption that the laser beam is passing just twice through the polymer layer. However, if the reflectance of the semiconductor electrode is not negligible at the measurement wavelength, the electrodes system can behave as a Fabry-Perot resonator and the evaluation of the electro-optic coefficient obtained via the application of the simplified single pass model is wrong [46]. As most researchers are using indium tin oxide (ITO) as the semitransparent electrode, this means that, unless a deeper theoretical approach is used [45,47–49], all the measurements obtained for wavelengths larger than about 1μm are affected by large errors due to the fact that ITO has got its plasma resonance in near-infrared and becomes reflective. Better results can be obtained in the near-infrared region by using aluminium doped zinc oxide (ZnO:Al) or, alternatively, more transparent electrodes [50,51].

3.2. Second Harmonic Generation

Since the EO coefficient r is related with the second order susceptibility term $\chi^{(2)}$ (see Equation (14)) it is possible to evaluate it by measuring the efficiency of the second harmonic generation process in polymeric films. Second harmonic generation was the first all-optical phenomenon shown in an experiment in nonlinear optics [52]. The experiment consisted in focusing a ruby laser beam on a crystalline quartz plate and revealing the second harmonic with a prism spectrometer on a photographic plate. The conversion efficiency has greatly improved with respect to the first experiments and second harmonic generation is now ordinarily used in photonic devices and applications. Moreover, due to the fact that the $\chi^{(2)}$ coefficient is present only in non-centrosymmetric materials, SHG was widely used in order to study symmetry properties of bulk materials, thin films [53,54] or surfaces [55,56] with high sensitivity in terms of linear measurements [57,58].

Usually, the polymeric samples used in SHG measurements are film deposited by spin coating on glass substrates. In order to prevent influencing the measurement, the substrate was an amorphous glass slide (no $\chi^{(2)}$ contribution) without electrodes on the polymeric film. Since, after deposition, the orientation of the nonlinear chromophores is isotropic, the material must be poled before measurement. In this case, the poling technique used is the corona poling, as it does not require any contact electrode. An alternative poling procedure is the in-plane poling or lateral poling [59] where the electric field is

applied between two coplanar electrodes that are deposited on the polymeric surface beside the region where the SHG measurements are performed. In the case of using an electrode for contact poling, the analysis of the multilayer structure should be performed as in [60].

A standard technique used in order to measure the electro-optic coefficient by SHG from poled samples is the Maker fringes scheme [18–20] where second harmonic signal is detected as a function of the incidence angle α. The fundamental beam at the angular frequency ω is generated by a pulsed laser that can be suitably polarized (e.g., in s or p polarization state); likewise an analyzer selects either *s* or *p* polarization for the signal generated at 2ω. The power generated by the sample can be calculated by means of the theoretical expression for the SHG power [19] given by:

$$W_{2\omega}(\alpha) = \left(\frac{512\pi^3}{A}\right)(t_\omega(\alpha))^4 (T_{2\omega}(\alpha))W_\omega^2 \frac{(\sin(\Psi(\alpha)))^2}{\left[(n_\omega(\alpha))^2 - (n_{2\omega}(\alpha))^2\right]^2}(d_{eff}(\alpha))^2 \tag{30}$$

where A is the area of the transverse section of the fundamental beam, $T_{2\omega}$ is the intensity transmittance of the output film/air interface at 2ω, t_ω is the field transmission coefficient of the input air/glass interface at ω (neglecting the glass/film interface due to the small refractive index contrast), W_ω represents the input power of the fundamental beam, $n_\omega(\alpha)$ and $n_{2\omega}(\alpha)$ are the polarization dependent refractive indices at ω and 2ω and d_{eff} is the effective nonlinearity. The phase factor $\Psi(\alpha)$ is given by:

$$\Psi = \left(\frac{\pi L}{2}\right)\left(\frac{4}{\lambda}\right)(n_\omega(\alpha)\cos(\alpha'_\omega) - n_{2\omega}(\alpha)\cos(\alpha'_{2\omega})) \tag{31}$$

L being the sample thickness, α'_ω and $\alpha'_{2\omega}$ the internal refraction angles corresponding to ω and 2ω.

In the Equation (30), $d_{eff}(\alpha)$ is the effective nonlinearity term depending on the $\underline{\underline{d}}$ tensor components, the optical axes orientation with respect to the sample surface and the fundamental beam incidence angle α, where the d tensor is is related with the $\chi^{(2)}$ tensor by the relation

$$d_{ijk} = \tfrac{1}{2}\chi_{ijk}^{(2)} \tag{32}$$

The expression for $d_{eff}(\alpha)$ is generally rather complicated but it becomes significantly simplified for particular symmetries. Specifically, the $\underline{\underline{d}}$ tensor corresponding to a poled polymer presents only two nonzero different components, d_{33} and $d_{31} = d_{32} = d_{24} = d_{15}$. Depending on the polarization of both fundamental and generated beams, it is possible to retrieve separately the value of these components. The d_{31} component can be directly evaluated from SHG measurements obtained in the $s_\omega p_{2\omega}$ configuration, since in this case the expression of d_{eff} is given by:

$$d_{eff}^{s-p} = d_{31}\sin(\alpha_\omega) \tag{33}$$

where α_ω is the fundamental beam propagation angle in the nonlinear film. The d_{33} coefficient can be obtained from a $p_\omega p_{2\omega}$ SHG measurement, by using the d_{31} evaluated with an independent $s_\omega p_{2\omega}$ measurement, since d_{eff} in the $p_\omega p_{2\omega}$ case is given by:

$$d_{eff}^{p-p} = d_{31}\sin(2\alpha_\omega)\cos(\alpha_{2\omega}) + d_{31}\cos(\alpha_\omega)^2\sin(\alpha_{2\omega}) + d_{33}\sin(\alpha_{2\omega})\sin(\alpha_{2\omega})^2 \tag{34}$$

where $\alpha_{2\omega}$ is the SH beam propagation angle in the nonlinear film.

The previous procedure can be used to find the susceptibility coefficient $\chi_{ijk}^{(2)}(-2\omega,\omega,\omega)$ via the Equation (32). Then, in order to recover the electro-optic coefficient a modified expression of Equation (17) can be used [61,62]:

$$r_{33}(-\omega,\omega,0) = -\frac{f^0}{f^\omega}\frac{2}{n_\omega^4}\chi_{ijk}^{(2)}(-2\omega,\omega,\omega) \tag{35}$$

where the field factors Equations (7) and (8) are present. We point out that in the two-index simplified notation, d_{ij} is proportional to r_{ji}. SHG measurement evaluates independently d_{31} and d_{33}, so the technique can be used to check the ratio $\frac{r_{33}}{r_{13}} = \frac{d_{33}}{d_{31}}$ and, indirectly, verify if the assumption $r_{33} \approx 3r_{13}$, used in the nonlinear ellipsometric technique is valid. By continuously measuring the SHG signal, it is possible to perform faster measurements that can be usefully used in monitoring the time decay of the electro-optic coefficient as we will show later.

3.3. Temperature Scanning Technique

In order to retrieve preliminary information on the stability of the induced electro-optic coefficient, temperature scanning measurements were performed. This type of measurement consists of the continuous measurement of the electro-optic coefficient of a poled sample while the temperature is increased from room temperature up to temperatures above T_g at a fixed rate, typically ranging between 1 °C/min to 5 °C/min.

During the temperature scanning procedure, the polymer electro-optic coefficient quickly relaxes and it is not stable enough to allow the use of the complete ellipsometric technique or the complete Maker fringe technique. In this case, the faster measurements shown previously (at the end of the Section 3.1, 3.2 paragraph) are preferred. The sample must be poled as usual and cooled down to room temperature, then the sample is gradually heated to the glass transition temperature (T_g), while the electro-optic coefficient is continuously monitored (by using either fast TMT or fast SHG). At the end of the measurements, the r_{33} is evaluated as a function of the temperature. Typical graphs are given by normalizing the r_{33} value with respect to the r_{33} coefficient measured at the beginning in room temperature condition. As an example, Figure 5 reports the measurement performed on a fluorinated electro-optic polymer [62], the HFIP-DR1AF that we will investigate more extensively in the fourth chapter. It is clear that the electro-optic coefficient remains stable up to a certain temperature, then decreases down to zero when the sample is heated close to T_g. It is possible to define a depolarization temperature (T_{dep}) as the temperature at which r_{33} gets half of the initial maximum value at room temperature. In this case, T_{dep} represents an indication of the stability of chromophore orientation in the polymer matrix.

It is evident that it is possible to compare different polymer types with this technique only if all the measurements are performed under the same conditions, *i.e.*, with the same temperature scanning rate.

Figure 5. Temperature scanning measurement on HFIP-DR1AF. Reprinted with permission from [62]. Copyright 2005, American Institute of Physics.
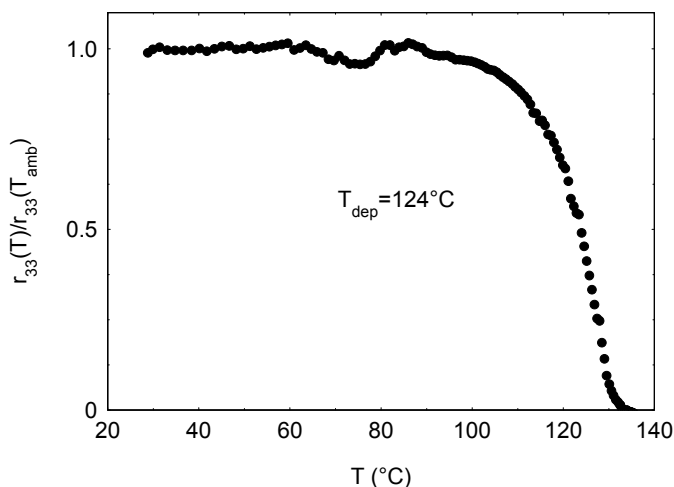
3.4. Isothermal Relaxation Measurements

A more reliable and useful measurement technique to probe stability of the EO properties is the series of isothermal relaxation measurements. In this technique, the sample must be poled, as usual, at the poling temperature T_p for a time interval Δt_p with an applied poling voltage V_p, then the sample is cooled down to the measurement temperature T_m maintaining the applied poling field. As soon as the T_m is reached, the poling field is switched off and the EO coefficient is continuously monitored by using either fast TMT or fast SHG measurements. In this case, the value of r_{33} is evaluated as a function of time for the given temperature T_m. As an example, Figure 6 reports the isothermal measurements at 90 °C, 110 °C, 130 °C (in log scale in this example) performed on HFIP-DR1AF [62].

Figure 6. Isothermal relaxation measurements on HFIP-DR1AF. Reprinted with permission from [62].Copyright 2005, American Institute of Physics.
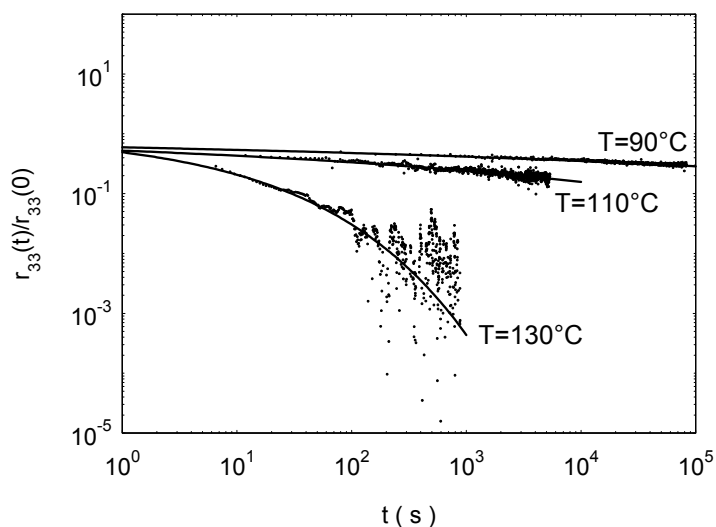

Aligning the behaviour of the EO coefficient with the Kohlrausch-Williams-Watts (KWW) stretched exponential law Equation (20), it is possible to obtain the value of the time constant τ, of the

stretching constant β and, from Equation (21), the value of the average time constant <τ> at a given temperature.

By comparing the curves for different temperatures, it is possible to retrieve the dependence of β and <τ> as a function of temperature. The β dependence is usually described by the Equation (24), while <τ> is well described by the Equation (22) for temperatures close or greater than T_0, and by the Equation (23) for temperatures below T_0. In Figure 7, we report the <τ> values obtained in the previous measurements in logarithmic scale as a function of the reciprocal of the absolute temperature (multiplied by 1,000), as is usually done when describing temperature activated processes [62].

Figure 7. Plot of the average relaxation-time constant retrieved from the measurements similar to the one reported in Figure 6. Reprinted with permission from [62].Copyright 2005, American Institute of Physics.
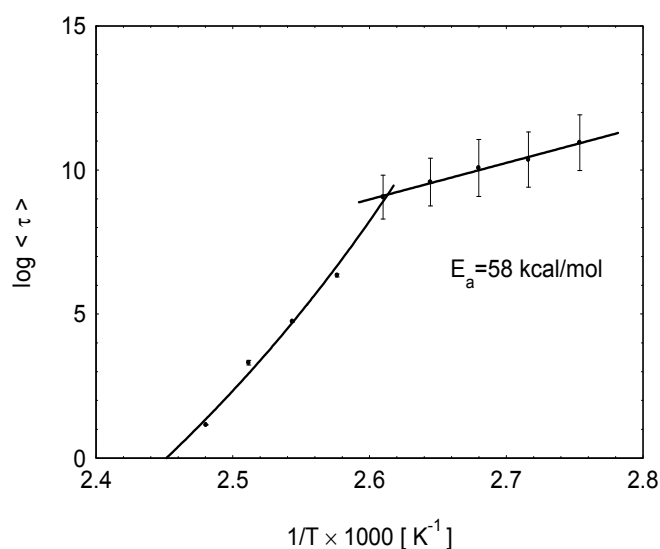
For temperatures below $T_0 \approx 110$ °C, (1/T × 1,000 > 2.6 K^{-1}), the average time constant follows an Arrhenius behaviour Equation (23). The Arrhenius behavior is described by a straight line in such type of plot. an activation energy E_a = 58 kcal/mol is then obtained by fitting the measurements below 110 °C with the Equation (23). For temperatures above 110 °C the relaxation is faster than that predicted by the Arrhenius model and follows the Vogel-Fulcher-Tamann-Hesse (VFTH) behavior (or Williams-Landel-Ferry (WLF)) described in the Equation (22). The activation energy is a parameter that represents the stability of the chromophores orientation in a more complete way than the depolarization temperature reported in the previous paragraph. Moreover, the activation energy can be recovered by performing measurements at relatively high temperatures, and can be used to extrapolate time constants at a lower temperature (room temperature) that cannot easily be measured (because it would take years).

We point out that, for this purpose, it is necessary to be sure that the measurements are performed in the Arrhenius regime and not in the VFTH regime. This last observation shows that it is not possible to perform relaxation measurements at high temperatures, near T_g, (appealing for their convenience, as they are rather quick measurements) in order to extrapolate the relaxation time constants at a low temperature (e.g., 50 °C) by using an Arrhenius type model. From the activation energy E_a, by using Equation (23), it is possible to estimate another stability parameter, the one-year stability working

temperature (T^{1yr}) that is the working temperature corresponding at an average time constant of one year.

4. Stability of Some Fluorinated Polymers

Here we show the results of the measurements described above on different fluorinated and non fluorinated electro-optic polymer species that are present in literature. The first four cases regard EO fluorinated polymers that can be used directly in the fabrication of active waveguides, meanwhile the other cases, here presented, are very stable crosslinkable EO polymers that can be used in EO modulators coupled with passive fluorinated waveguides [63].

4.1. HFIP-DR1AF

The copolymer described here is a fluorinated side-chain copolymer, the HFIP-DR1AF [62], with Tg = 130 °C, whose structure is described in Figure 8(a). It is an evolution of the well-known poly(methylmethacrylate) bearing the DR1 chromophore (DR1PMMA), with structure shown in Figure 8(b), where a part of the C-H groups was substituted with C-F.

Figure 8. (**a**) chemical structure of the HFIP-DR1AF; (**b**) chemical structure of the DR1PMMA. Reprinted with permission from [62]. Copyright 2005, American Institute of Physics.

(**a**) (**b**)
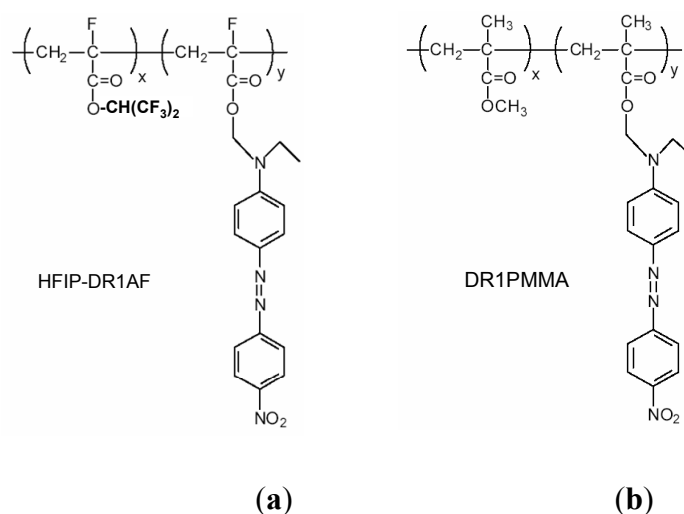
The synthesis of the copolymers was carried out with the hexafluoroisopropyl alphafluoroacrylate monomer (HFIPAF) and the alphafluoroacrylate monomer bearing the Disperse Red 1 (DR1) chromophore (DR1AF). The polymer present 46 % of DR1 substituted group, the electro-optic coefficient of the sample was measured at $\lambda = 1{,}550$ nm, resulting to be $r_{33} = (4.6 \pm 0.5)$ pm/V, for a poling field of $E_p = 43$ V/μm.

Thermal stability of the poling induced electro-optic coefficient was measured by means of both temperature scanning and isothermal relaxation measurements as shown in Figures 5–7. We scanned the temperature from the ambient one up to 140 °C, above the T_g, at the rate $dT/dt = 5$ °C/min. From Figure 5 it results a depolarization temperature $T_{dep} = 124$ °C, close to, but lower than, the polymer glass-transition temperature T_g.

We then performed isothermal relaxation measurements (Figure 6) for different temperatures ranging between 90 °C and 130 °C. The retrieved activation energy is $E_A \approx 58$ kcal/mol.

4.2. FATRIFE-DR1AF

The copolymer described here is a fluorinated side-chain copolymer, the FATRIFE-DR1AF [64] with $T_g = 112$ °C, whose structure is similar to the one described in Figure 8(a) except that the side group $-CH(CF_3)_2$ is substituted by the side group $-CH_2CF_3$. It is an evolution of DR1PMMA, with structure shown in Figure 8b, where a part of the C-H groups was substituted with C-F. The polymer constitute 30% of the DR1 substituted group; the electro-optic coefficient of the sample was measured at $\lambda = 1550$ nm, resulting to be $r_{33} = (4.7 \pm 0.5)$ pm/V, for a poling field of $E_p = 48$ V/µm.
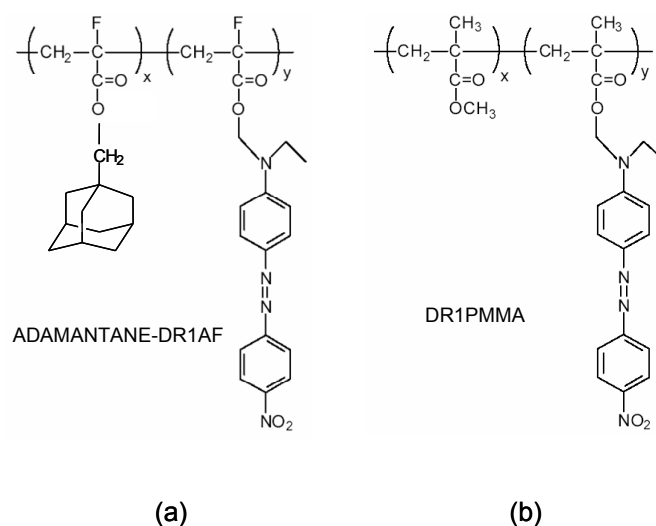
Thermal stability of the poling induced electro-optic coefficient was measured by means of both temperature scanning and isothermal relaxation measurements [64]. We scanned the temperature from the ambient one up to 140 °C, above the T_g, at the rate $dT/dt = 5$ °C/min. The resulting depolarization temperature $T_{dep} = 114$ °C, close to, but lower than, the polymer glass-transition temperature T_g.

We then performed isothermal relaxation measurements for different temperatures ranging between 60 °C and 110 °C. The retrieved activation energy is $E_A \approx 60$ kcal/mol.

4.3. ADAMANTANE-DR1AF

The copolymer described here is a fluorinated side-chain copolymer, the ADAMANTANE-DR1AF [11] with $T_g = 148$ °C. The synthesis of the copolymer was carried out with a molar fraction $x = 73\%$ of the α-fluoroacrylate monomer bearing a heavy stabilizing diamond-like side group, the adamantane ($-CH_2-C_{10}H_{15}$), and a molar fraction y = 27% of the α-fluoroacrylate monomer bearing the Disperse Red 1 (DR1) chromophore (DR1AF). The general structure is given in Figure 9(a). Also the ADAMANTANE-DR1AF is an evolution of the DR1PMMA (Figure 9(b)) [11], where a part of the C-H groups was substituted with C-F and with the adamantane as a supplementary side group.

Figure 9. (**a**) chemical structure of the ADAMANTANE-DR1AF; (**b**) chemical structure of the DR1PMMA. Reprinted with permission from [11]. Copyright 2006, American Institute of Physics.

(a)   (b)

The electro-optic coefficient of the sample fabricated with ADAMANTANE-DR1AF was measured at $\lambda = 1{,}550$ nm and it becomes $r_{33} = (2.8 \pm 0.3)$ pm/V, for a poling field of $E_p = 43$ V/µm.

Thermal stability of the poling induced electro-optic coefficient was measured by means of both temperature scanning and isothermal relaxation measurements [11].

We scanned the temperature from the ambient one up to 150 °C, above the T_g, at a constant rate $\Delta T/\Delta t = 5$ °C/min. In Figure 10, the results obtained for the ADAMANTANE-DR1AF copolymer is shown. From the measurements, the results show $T_{dep} = 136$ °C, close to, but lower than, the polymer glass-transition temperature T_g.

Figure 10. Temperature scanning measurements on ADAMANTANE-DR1AF. Reprinted with permission from [11]. Copyright 2006, American Institute of Physics.
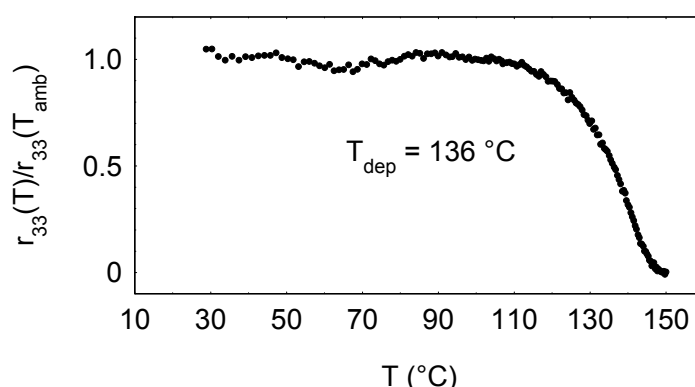

We then performed isothermal relaxation measurements on the ADAMANTANE-DR1AF sample for different temperatures ranging between 110 °C and 140 °C. In Figure 11 we show the isothermal relaxation of the EO coefficient normalized to the initial value $r_{33}(t)/r_{33}(0)$, for the three different fluorinated compounds presented so far, performed at the same temperatures $T_m = 110$ °C. The increase of the thermo-stability of the ADAMANTANE-DR1AF copolymer with respect to the other species is evident.

Figure 11. Isothermal relaxation measurements at $T_m = 110$ °C for three fluorinated copolymers: ADAMANTANE-DR1AF, FATRIFE-DR1AF, and HFIP-DR1AF . Reprinted with permission from [11]. Copyright 2006, American Institute of Physics.
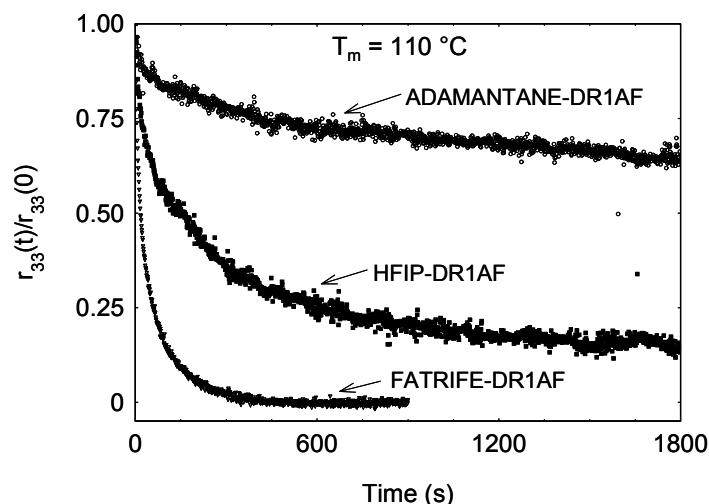
In Figure 12, we plot the values of log<τ> *vs.* 1000/T for the ADAMANTANE-DR1AF copolymer. The graph shows that relaxation of the chromophores orientation can be described by the Arrhenius law with activation energy $E_A \approx 105$ kcal/mol. This result must be compared with the value $E_A \approx 58$ kcal/mol obtained for the HFIP-DR1AF [62] and $E_A \approx 60$ kcal/mol for the FATRIFE-DR1AF [64]). This high activation energy, together with the high T_{dep}, leads to a high thermo-stability of the EO properties even at a high operative temperature, compared with other similar fluorinated DR1 based compounds.

Figure 12. Arrhenius plot of the average relaxation time constants retrieved from the isothermal relaxation measurements performed on the ADAMANTANE-DR1AF copolymer at different temperatures. Reprinted with permission from [11]. Copyright 2006, American Institute of Physics.
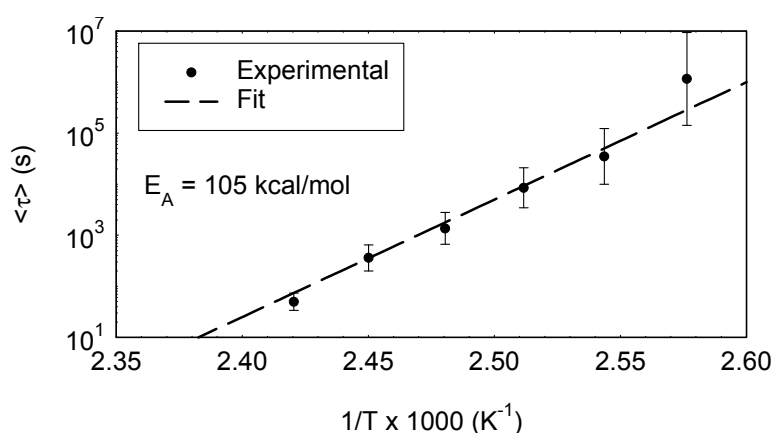
4.4. Polyimides-EHNT

The copolymer described here [65] is a fluorinated side-chain copolymer formed by a backbone of polyimides, whose synthesis was carried out by following the procedure in [65] with a 43% concentration in weight of 2-[4'-(N-ethyl-N-2-hydroxyethyl)-amino-phenylazo]-5-nitrothiazole (EHNT) of the chromophore side group [65]. The EHNT chromophore show a larger second order hyperpolarizability with respect to the DR1 chromophore shown previously. The Polyimides-EHNT shows a very high glass transition temperature of $T_g = 200$ °C.

The electro-optic coefficient of a sample fabricated with Polyimides-EHNT was measured at $\lambda = 1,550$ nm, resulting in $r_{33} = 18$ pm/V, after a corona poling procedure of one hour with an applied voltage of 8.5 kV at 190 °C.

Thermal stability of the poling induced electro-optic coefficient was measured by means of isothermal relaxation measurements performed at 80 °C and 120 °C, showing that at 120 °C the poled polymer maintains the 84% of its original r_{33} value after 200 h [65].

4.5. Phenyltetraenic and AJL8 in Antrhracene Crosslinkable Matrix

In [66], three different types of acrylate functionalized dendritic nonlinear optical chromophores were dispersed in high-Tg temperature anthracene crosslinkable matrix. The synthesis of the guest-host system was carried out by following the procedure in [66] with a chormophore concentration of about 17% in weight. The glass transition temperature of the host matrix (labelled P2 in [66]) is

exceptionally high T_g = 215 °C, meanwhile the Tg of the chromophores (labeled C1, C2, C3) ranges from 84 °C to 102 °C.

The electro-optic coefficient of the P2/C3 sample is the highest one with a value of r_{33} = 126 pm/V (measured at λ = 1,310 nm) after a poling procedure at 185 °C.

Thermal stability of the poling induced electro-optic coefficient was measured by means of TMT isothermal relaxation measurements performed at 150 °C, showing that the poled polymer maintains 88% of its original r_{33} value after 500 h [66].

4.6. FTC-EGDMA

The polymer described in [10] is a side-chain copolymer formed with 38% of the weight of the chromophore denoted in FTC [10] linked to a crosslinkable matrix formed by methylmethacrylate (MMA), dimetyl-azobisisobuthlate (MAIB) and methacryloyloxyyetyl isocyanata (MOI). The glass transition temperature results show T_g = 170 °C, and the electro-optic coefficient measured at λ = 1,310nm is 139 pm/V. By performing isothermal relaxation measurements at 85 °C, the poled polymer maintains 83% of its original r_{33} value after 500 h.

5. Conclusions

Electro-optic fluorinated copolymers are very useful materials for technological applications in the telecommunication domain. The presence of fluorine reduces optical losses at the telecom wavelength of 1,550 nm. Meanwhile, the electro-optic coefficient can be optimized by using suitable nonlinear chromophores, as appeared here as an example with the well-known Disperse Red 1 (DR1) and also the hetarylazo EHNT chromophore that presents a larger electro-optic coefficient and other chromophores. In this context, the time stability of the externally induced electro-optic coefficient is an important issue in technological design and can be optimized by developing a crosslinkable high-Tg polymers host. Here, we have shown different measurement techniques that can be utilized in the characterization of the time stability of the EO coefficient. A review of the application of these techniques to different copolymer species was given, showing the high potentiality of the fluorinated EO copolymers in this field of application.

References

1. Zyss, J. *Molecular Nonlinear Optics*. Academic Press Inc.: San Diego, CA, USA, 1994.
2. Rousseau, A.; Boutevin, B. Synthesis and characterization of organic materials for integrated optical devices. *AIP Conf. Proc.* **2003**, *709*, 214–232.
3. Pyayt, A.L. Guiding light in electro-optic polymers. *Polymers* **2011**, *3*, 1591–1599.
4. Oh, M.-C.; Kim, K.-J.; Chu, W.-S.; Kim, J.-W.; Seo, J.-K.; Noh, Y.-O.; Lee, H.-J. Integrated photonic devices incorporating low-loss fluorinated polymer materials. *Polymers* **2011**, *3*, 975–997.

5. Lee, M.; Katz, H.E.; Erben, C.; Gill, D.M.; Gopalan, P.; Heber, J.D.; McGee, D.J. Broadband modulation of light by using an electro-optic polymer. *Science* **2002**, *298*, 1401–1403.

6. Sun, H.; Chen, A.; Olbricht, B.C.; Davies, J.A.; Sullivan, P.A.; Liao, Y.; Dalton, L.R. Direct electron beam writing of electro-optic polymer microring resonators. *Opt. Express* **2008**, *16*, 6592–6599.

7. Sun, H.; Chen, A.; Olbricht, B.C.; Davies, J.A.; Sullivan, P.A.; Liao, Y.; Dalton, L.R. Microring resonators fabricated by electron beam bleaching of chromophore doped polymers. *Appl. Phys. Lett.* **2008**, *92*, 193305:1–193305:3.

8. Song, H.-C.; Oh, M.-C.; Ahn, S.-W.; Steier, W.H.; Fetterman, H.R.; Zhang C. Flexible low-voltage electro-optic polymer modulators . *Appl. Phys. Lett.* **2003**, *82*, 4432–4434.

9. Belardini, A.; Larciprete, M.C.; Cianci, E.; Foglietti, V.; Ratsimihety, A.; Rousseau, A.; Michelotti, F. Direct E-beam writing of electro-optic polymer channel waveguides. *AIP Conf. Proc.* **2003**, *709*, 427–428.

10. Mori, Y.; Nakaya, K.; Piao, X.; Yamamoto, K.; Otomo, A.; Yokoyama, S. Large electro-optic activity and enhanced temporal stability of methacrylate-based crosslinking hyperbranched nonlinear optical polymer. *J. Polym. Sci. A Polym. Chem.* **2012**, *50*, 1254–1260.

11. Belardini, A.; Dominici, L.; Larciprete, M.C.; Michelotti, F.; Rousseau, A.; Ratsimihety, A. Enhanced stability of the second order optical properties of high-Tg fluorinated electro-optic copolymer. *Appl. Phys. Lett.* **2006**, *89*, 231110:1–231110:3.

12. Pliška, T.; Cho, W.-R.; Meier, J.; Le Duff, A.-C.; Ricci, V.; Otomo, A.; Canva, M.; Stegeman, G.I.; Raimond, P.; Kajzar, F. Comparative study of nonlinear-optical polymers for guided-wave second-harmonic generation at telecommunication wavelengths. *J. Opt. Soc. Am. B* **2000**, *17*, 1554–1564.

13. Teng, C.C.; Man, H.T. Simple reflection technique for measuring the electro-optic coefficient of poled polymers. *Appl. Phys. Lett.* **1990**, *56*, 1734–1736.

14. Schildkraut, J.S. Determination of the electrooptic coefficient of a poled polymer film. *Appl. Opt.* **1990**, *29*, 2839–2841.

15. Michelotti, F.; Nicolao, G.; Tesi, F.; Bertolotti, M. On the measurement of the electro-optic properties of poled side-chain copolymer films with a modified Teng-Man technique. *Chem. Phys.* **1999**, *245*, 311–326.

16. Dominici, L.; Michelotti, F.; Whitelegg, S.; Campbell, A.; Bradley, D.D.C. Comparative study of space-charge effects in polymer light emitting diodes by means of reflection electro-optic and electroabsorption techniques. *Phys. Rev. B* **2004**, *69*, 054201:1–054201:10.

17. Yariv, A. *Optical Electronics*, 4th ed.; Saunders College Publishing: Philadelphia, PA, USA, 1991.

18. Maker, P.D.; Terhune, R.W.; Nisenhoff, M.; Savage, C.M. Effects of dispersion and focusing on the production of optical harmonics. *Phys. Rev. Lett.* **1962**, *8*, 21–22.

19. Jerphagnon, J.; Kurtz, S.K. Maker fringes: a detailed comparison of theory and experiment for isotropic and uniaxial crystals. *J. Appl. Phys.* **1970**, *41*, 1667–1681.

20. Herman, W.N.; Hayden, L.M. Maker fringes revisited: second-harmonic generation from birefringent or absorbing materials. *J. Opt. Soc. Am. B* **1995**, *12*, 416–427.

21. Bloembergen, N. *Nonlinear Optics*, 4th ed.; World Scientific Publication Co. Pte. Ltd.: River Edge, NJ, USA, 1996.

22. Fazio, E.; Ramadan, W.; Belardini, A.; Bosco, A.; Bertolotti, M.; Petris, A.; Vlad, V.I. (2+1)D vortex soliton-like propagation in photorefractive $Bi_{12}SiO_{20}$ crystals, *Phys. Rev. E* **2003**, *67*, 026611:1–026611:8.

23. Singer, K.D.; Kuzyk, M.G.; Sohn, J.E. Second-order nonlinear-optical processes in orientationally ordered materials: relationship between molecular and macroscopic properties. *J. Opt. Soc. Am. B* **1987**, *4*, 968–976.

24. Harper, A.W.; Sun, S.; Dalton, L.R.; Garner, S.M.; Chen, A.; Kalluri, S.; Steier, W.H.; Robinson, B.H. Translating microscopic optical nonlinearity into macroscopic optical nonlinearity: the role of chromophore chromophore electrostatic interactions. *J. Opt. Soc. Am. B* **1998**, *15*, 329–337.

25. Cheng, L.T.; Tam, W.; Stevenson, S.H.; Meredith, G.R.; Rikken, G.; Marder, S.R. Experimental investigations of organic molecular nonlinear optical polarizabilities. 1. Methods and results on benzene and stilbene derivatives. *J. Phys. Chem.* **1991**, *95*, 10631–10643.

26. Cheng, L.T.; Tam, W.; Stevenson, S.H.; Meredith, G.R.; Rikken, G.; Marder, S.R. Experimental investigations of organic molecular nonlinear optical polarizabilities. 2. A study of conjugation dependences. *J. Phys. Chem.* **1991**, *95*, 10643–10652.

27. Dalton, L.R.; Steier, W.H.; Robinson, B.H.; Zhang, C.; Ren, A.; Garner, S.; Chen, A.; Londergan, T.; Irwin, L.; Carlson, B.; Fifield, L.; Phelan, G.; Kincaid, C.; Amend, J.; Jen, A. From molecules to opto-chips: Organic electro-optic materials. *J. Mater. Chem.* **1999**, *9*, 1905–1920.

28. Dalton, L.; Harper, A.; Ren, A.; Wang, F.; Todorova, G.; Chen, J.; Zhang, C.; Lee, M. Polymeric electro-optic modulators: From chromophore design to integration with semiconductor very large scale integration electronics and silica fiber optics. *Ind. Eng. Chem. Res.* **1999**, *38*, 8-33.

29. Moylan, C.R.; Twieg, R.J.; Lee, V.Y.; Swanson, S.A.; Betterton, K.M.; Miller, R.D. Nonlinear optical chromophores with large hyperpolarizabilities and enhanced thermal stabilities. *J. Am. Chem. Soc.* **1993**, *115*, 12599–12600.

30. Skinner, I.M.; Garth, S.J. Reconciliation of esu and mksa units in nonlinear optics. *Am. J. Phys.* **1990**, *58*, 177–181.

31. Blanchard, D.M.; Mitchell, G.R. A comparison of photoinduced poling and thermal poling of azo-dye-doped polymer films for second order nonlinear optical applications. *Appl. Phys. Lett.* **1993**, *63*, 2038–2040.

32. Bauer-Gogonea, S.; Bauer, S.; Wirges, W.; Gerhard-Multhaupt, R. Pyroelectrical investigation of the dipole orientation in nonlinear optical polymers during and after photoinduced poling. *J. Appl. Phys.* **1994**, *76*, 2627–2635.

33. Wu, J.W. Birefringent and electro-optic effects in poled polymer films: Steady-state and transient properties. *J. Opt. Soc. Am. B* **1991**, *8*, 142–152.

34. Michelotti, F.; Toussaere, E. Pulse poling of side-chain and crosslinkable copolymers. *J. Appl. Phys.* **1997**, *82*, 5728–5744.

35. Brasselet, S.; Zyss, J. Multipolar molecules and multipolar fields: Probing and controlling the tensorial nature of nonlinear molecular media. *J. Opt. Soc. Am. B* **1998**, *15*, 257–288.

36. Quatela, A.; De Matteis, F.; Casalboni, M.; Stella, F.; Colombo, M.; Zaopo, A. Order relaxation of a poled azo dye in a high Tg, fully aromatic polyimide. *J. Appl. Phys.* **2007**, *101*, 023116:1–023116:6.

37. Scher, H.; Shlesinger, M.F.; Bendler, J.T. Time scale invariance in transport and relaxation. *Phys. Today* **1991**, *44*, 26–34.

38. Williams, G.; Watts, D.C. Non-symmetrical dielectric relaxation behaviour arising from a simple empirical decay function. *Trans. Faraday Soc.* **1970**, *66*, 80–85.

39. Ghebremichael, F.; Kuzyk, M.G. Optical second-harmonic generation as a probe of the temperature dependence of the distribution of sites in a poly(methyl methacrylate) polymer doped with disperse red 1 azo dye. *J. Appl. Phys.* **1995**, *77*, 2896–2901.

40. Michelotti, F.; Taggi, V.; Bertolotti, M.; Gabler, T.; Hörhold, H.H.; Bräuer, A. Reflection electro-optical measurements on electroluminescent polymer films: A good tool for investigating charge injection and space charge effects. *J. Appl. Phys.* **1998**, *83*, 7886–7895.

41. Michelotti, F.; Bussi, S.; Dominici, L.; Bertolotti, M.; Bao, Z. Space charge effects in polymer-based light-emitting diodes studied by means of a polarization sensitive electroreflectance technique. *J. Appl. Phys.* **2002**, *91*, 5521–5532.

42. Miniewicz, A.; Michelotti, F.; Belardini, A. Photoconducting polymer-liquid crystal structure studied by electroreflectance. *J. Appl. Phys.* **2004**, *95*, 1141–1147.

43. Michelotti, F. Dominici, L. Belardini, A. Charge injection and trapping contributions to the electro-optic response of mesoscopic polymer systems. *AIP Conf. Proc.* **2003**, *709*, 233–251.

44. Jespersen, K.G.; Pedersen, T.G.; Johansen, P.M. Electro-optic response of chromophores in a viscoelastic polymer matrix to a combined dc and ac poling field. *J. Opt. Soc. Am. B* **2003**, *20*, 2179–2188.

45. Nagtegaele, P.; Brasselet, E.; Zyss, J. Anisotropy and dispersion of a Pockels tensor: A benchmark for electro-optic organic thin-film assessment. *J. Opt. Soc. Am. B* **2003**, *20*, 1932–1936.

46. Michelotti, F.; Belardini, A.; Larciprete, M.C.; Bertolotti, M.; Rousseau, A.; Ratsimihety, A.; Schoer, G.; Mueller, J. Measurement of the electro-optic properties of poled polymers at $\lambda = 1.55\,\mu m$ by means of sandwich structures with zinc oxide transparent electrode. *Appl. Phys. Lett.* **2003**, *83*, 4477–4479.

47. Park, D.H.; Lee, C.H.; Herman, W.N. Analysis of multiple reflection effects in reflective measurements of electro-optic coefficients of poled polymers in multilayer structures. *Opt. Express* **2006**, *14*, 8866–8884.

48. Hou, A.; Liu, H.; Sun, J.; Zhang, D.; Yi, M. Measurement of the electro-optic coefficient of polymer thin films with better spatial resolution. *Optics & Laser Tech.* **2007**, *39*, 411–414.

49. Park, D.H.; Luo, J.; Jen, A.K.-Y.; Herman, W.N. Simplified reflection Fabry-Perot method for determination of electro-optic coefficients of poled polymer thin films. *Polymers* **2011**, *3*, 1310–1324.

50. Michelotti, F.; Belardini, A.; Rousseau, A.; Ratsimihety, A.; Schoer, G.; Muller, J. Use of sandwich structures with ZnO:Al transparent electrodes for the measurement of the electro-optic properties of standard and fluorinated poled copolymers at $\lambda = 1.55$ μm. *J. Non-Crystalline Solids* **2006**, *352*, 2339–2342.

51. Michelotti, F.; Canali, R.; Dominici, L.; Belardini, A.; Menchini, F.; Schoer, G.; Muller, J. Second order optical nonlinearity of ZnO/ZnO:Al bilayers deposited on glass by low temperature radio frequency sputtering. *Appl. Phys. Lett.* **2007**, *90*, 181110:1–181110:3.

52. Franken, P.A.; Hill, A.E.; Peters, C.W.; Weinreich, G. Generation of optical harmonics. *Phys. Rev. Lett.* **1961**, *7*, 118–119.

53. Cattaneo, S.; Kauranen, M. Determination of second-order susceptibility components of thin films by two-beam second-harmonic generation. *Opt. Lett*. **2003**, *28*, 1445–1447.

54. Larciprete, M.C.; Bovino, F.A.; Giardina, M.; Belardini, A.; Centini, M.; Sibilia, C.; Bertolotti, M.; Passaseo, A.; Tasco, V. Mapping the nonlinear optical susceptibility by noncollinear second-harmonic generation. *Opt. Lett.* **2009**, *34*, 2189–2191.

55. Verbiest, T.; Kauranen, M.; Van Rompaey, Y.; Persoonson, A. Optical activity of anisotropic achiral surfaces. *Phys. Rev. Lett.* **1996**, *77*, 1456–1459.

56. Belardini, A.; Larciprete, M.C.; Centini, M.; Fazio, E.; Sibilia, C.; Chiappe, D.; Martella, C.; Toma, A.; Giordano, M.; Buatier de Mongeot, F. Circular dichroism in the optical second-harmonic emission of curved gold metal nanowires. *Phys. Rev. Lett.* **2011**, *107*, 257401:1–257401:5.

57. Verbiest, T.; Clays, K.; Rodriguez, V. *Second-Order Nonlinear Optical Characterization Techniques*. CRC Press, NY, USA, 2009.

58. Belardini, A.; Pannone, F.; Leahu, G.; Larciprete, M.C.; Centini, M.; Sibilia, C.; Martella, C.; Giordano, M.; Chiappe, D.; Buatier de Mongeot, F. Evidence of anomalous refraction of self-assembled curved gold nanowires, *Appl. Phys. Lett.* **2012**, *100*, 251109:1–251109:5.

59. Palazzesi, C.; Stella, F.; de Matteis, F.; Casalboni, M. In-plane poling characterization of organic electro-optical polymer. *J. Appl. Phys.* **2010**, *107*, 113101:1–113101:5.

60. Park, D.H.; Herman, W.N. Closed-form Maker fringe formulas for poled polymer thin films in multilayer structures. *Opt. Express* **2012**, *20*, 173–185.

61. Large, M.J.; Kajzar, F.; Raimond, P. Modulation of second harmonic generation in photochromic materials by the application of electric fields and low intensity light. *Appl. Phys. Lett.* **1998**, *73*, 3635–3637.

62. Belardini, A.; Larciprete, M.C.; Passeri, D.; Michelotti, F.; Ratsimihety, A.; Rousseau, A.; Menchini, F.; Nichelatti, E. Concentration dependence of the optical nonlinearity in extremely doped fluorinated organic copolymers. *J. Appl. Phys.* **2005**, *98*, 093521:1–093521:8.

63. Ahn, S.-W.; Steier, W.H.; Kuo, Y.-H.; Oh, M.-C.; Lee, H.-J.; Zhang, C.; Fetterman, H.R. Integration of electro-optic polymer modulators with low-loss fluorinated polymer waveguides. *Opt. Lett.* **2002**, *27*, 2109–2111.

64. Belardini, A.; Michelotti, F.; Rousseau, A.; Ratsimihety, A. Temperature stability of the electro-optic response of highly fluorinated side chain organic copolymers. *Ferroelectrics* **2007**, *352*, 35–41.

65. He, M.; Zhou, Y.; Dai, J.; Liu, R.; Cui, Y.; Zhang, T. Synthesis and nonlinear optical properties of soluble fluorinated polyimides containing hetarylazo chromophores with large hyperpolarizability. *Polymer* **2009**, *50*, 3924–3931.

66. Shi, Z.; Luo, J.; Huang, S.; Polishak, B.M.; Zhou, X.-H.; Liff, S.; Younkin, T.R.; Block, B.A.; Jen, A.K.-J. Achieving excellent electro-optic activity and thermal stability in poled polymers through an expeditious crosslinking process. *J. Mater. Chem.* **2012**, *22*, 951–959.